Magnetic and transport properties of $SrFeO_x$

G. V. M. Williams,[1] E. K. Hemery,[1,2] and D. McCann[1]
[1]*MacDiarmid Institute for Advanced Materials and Nanotechnology, Industrial Research, P.O. Box 31310, Lower Hutt 5040, New Zealand*
[2]*MacDiarmid Institute for Advanced Materials and Nanotechnology, Victoria University, Wellington 6140, New Zealand*
(Received 6 August 2008; published 12 January 2009)

We report the results from magnetic and transport measurements on $SrFeO_x$ where we focus on oxygen contents about the $Sr_4Fe_4O_{11}$ phase ($x=2.75$) that antiferromagnetically orders at ~230 K. We find an exchange-bias-like effect in $Sr_4Fe_4O_{11}$ that commences near the Fe(2) moment Néel temperature (~230 K). While there is a weak spin-glass component, possibly arising from spin-frustrated moments on the Fe(1) sites, the spin-glass temperature is significantly less than 230 K, and hence the exchange-bias-like effect is unlikely to be due to a spin glass. The exchange-bias-like effect clearly arises from an exchange interaction term that includes the Fe(2) spins but its exact nature is not clear and awaits a detailed theoretical study. Room-temperature thermopower measurements show a large change in sign for oxygen contents on either side of the $Sr_4Fe_4O_{11}$ phase, which we show can be qualitatively interpreted by assuming that the Fermi level is within a narrow band. High-field resistivity measurements show a large magnetoresistance that commences near the $Sr_4Fe_4O_{11}$ Néel temperature.

DOI: 10.1103/PhysRevB.79.024412 PACS number(s): 75.30.−m, 72.15.Jf

I. INTRODUCTION

$SrFeO_x$ has been shown to display interesting magnetic and electronic behavior and it is believed to be an inhomogeneous mixture of four phases for x ranging from 2.5 to 3.[1–3] The parent compound, $SrFeO_3$, is a cubic perovskite that has a metalliclike resistivity.[3–5] It is an antiferromagnet with a Néel temperature of $T_N=130$ K and a helical magnetic spin structure with the propagation vector parallel to the [111] direction. Decreasing the oxygen content below $x=3$ is initially believed to lead to a mixture of $SrFeO_3$ and $Sr_8Fe_8O_{23}$ ($x=2.875$).[2,5] The tetragonal $Sr_8Fe_8O_{23}$ phase [Fig. 1(a)] contains FeO_6 octahedra, distorted FeO_6 octahedra, and square pyramidal FeO_5.[6] It is an antiferromagnet with a Néel temperature of ~70 K.[2] It displays Verwey-type charge ordering that is evidenced by a jump in the resistivity below the Néel temperature.[1,2] There is also a large jump in the thermopower near this temperature that has been interpreted in terms of charge ordering on one of the Fe sites.[7]

Decreasing the oxygen content below 2.875 leads to the orthorhombic $Sr_4Fe_4O_{11}$ ($x=2.75$) phase [Fig. 1(b)] that contains square pyramidal $Fe(1)O_5$ and distorted $Fe(2)O_6$ octahedra.[6,8] It is believed to have a charge-ordering transition at ~675 K that results in equal amounts of Fe^{3+} and Fe^{4+}.[9] Hodges *et al.*[6] concluded that the Fe(1) valence is 4+ and the Fe(2) valence is 3+. However it has also been argued that $Fe^{3+}(1)$ and $Fe^{4+}(2)$ is a better assignment.[8,9] $Sr_4Fe_4O_{11}$ is semiconducting below the charge-ordering transition temperature where activation energies of 0.053 eV have been measured for $x=2.78$ and $x=2.72$.[10] This is consistent with band-structure calculations that deduce a band gap of 0.13 eV.[9] It is a *G*-type antiferromagnet with a Néel temperature of ~230 K, where the moments on the Fe(2) sites order antiferromagnetically and the Fe(1) site moments do not show long-range magnetic order.[6,8,9] The exchange interactions for the antiferromagnetically ordered Fe(2) moments are believed to be antiferromagnetic (AFM) Fe(2)-O-Fe(2) in the *ac* plane and Fe(2)-O-Fe(2) in the *b*-axis direction.[6,9] The Fe(1) moments are believed to be topologically spin frustrated due to a ferromagnetic (FM) Fe(1)-O-Fe(2) double-exchange interaction and Fe(1)-O-Fe(1) antiferromagnetic superexchange.[6,9] Decreasing the oxygen content below $x=2.75$ leads to orthorhombic $Sr_2Fe_2O_5$ ($x=2.5$) with Fe^{3+} as shown in Fig. 1(c).[6]

While the moments on the Fe(1) sites are not believed to magnetically order in $Sr_4Fe_4O_{11}$, it is not known if a spin glass exists and there are limited reports of transport measurements. For this reason we have performed a magnetic and transport study of $SrFeO_x$ with oxygen contents about the $Sr_4Fe_4O_{11}$ phase and report our results in this paper.

II. EXPERIMENTAL DETAILS

A series of polycrystalline $SrFeO_x$ samples was synthesized by solid-state reaction from stoichiometric mixtures of $Sr(NO_3)_2$ and Fe_2O_3. The sintering and annealing processes are described elsewhere.[7] The oxygen contents were estimated by first noting that the temperature-dependent magnetization of the as-made sample corresponds to published data for $x=2.95$. The samples were then annealed at different temperatures and oxygen partial pressures or in pure argon and then rapidly quenched into liquid nitrogen. The oxygen contents were then estimated from the mass differences. X-ray diffraction showed that the samples contained $SrFeO_x$ to within the limit of detectability. Temperature-dependent resistivity measurements were made at 0 and 12 T in a superconducting magnet using the four-terminal method. Magnetization measurements were made using a superconducting quantum interference device (SQUID) magnetometer. Room-temperature thermopower measurements were made using a standard differential temperature technique.

III. RESULTS AND ANALYSIS

The 6 T field-cooled magnetization data are plotted in Fig. 2 as M/H for oxygen contents of 2.80, 2.75, and 2.72. The

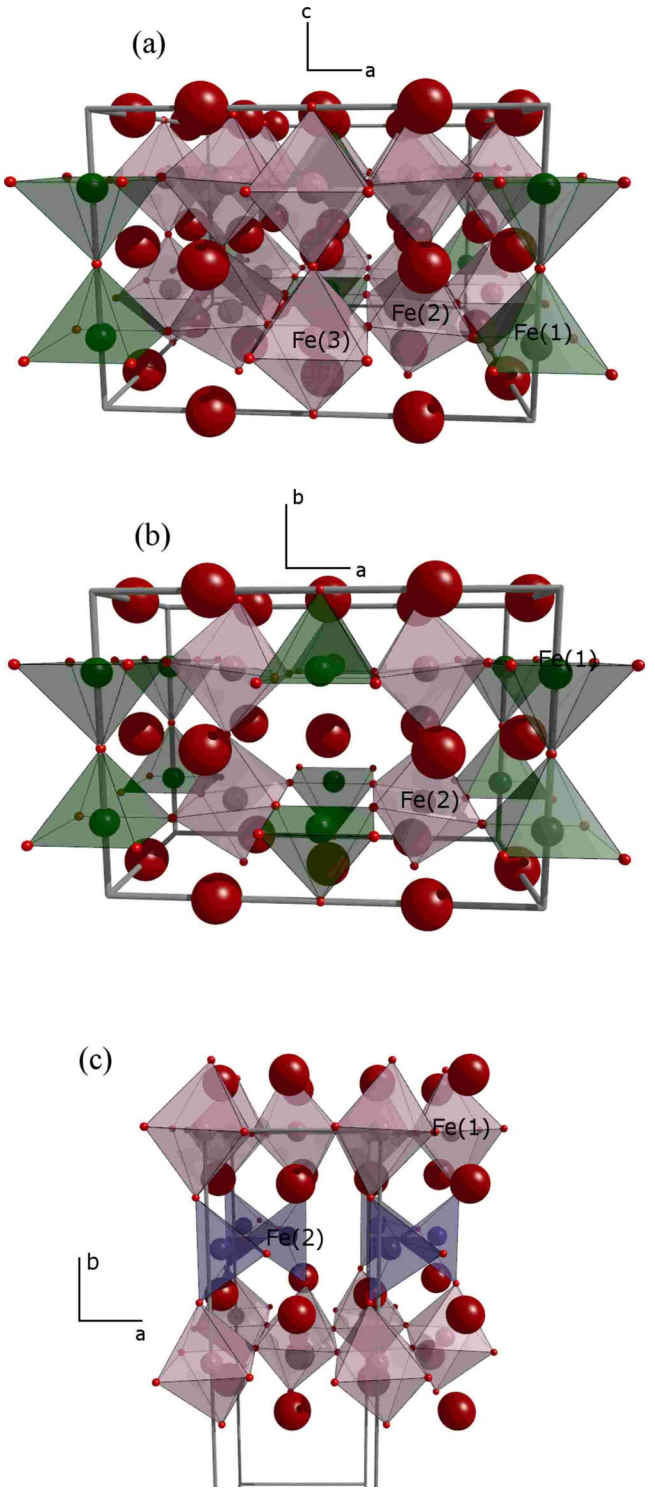

FIG. 1. (Color online) Crystal structures for the (a) tetragonal $Sr_8Fe_8O_{23}$ phase ($x=2.875$), (b) orthorhombic $Sr_4Fe_4O_{11}$ phase ($x=2.75$), and the (c) $Sr_2Fe_2O_5$ phase ($x=2.5$) (Ref. 6). Oxygen, Fe, and Sr are indicated by small, medium, and large spheres. The crystallographic axis are indicated where the b axis is out of the plane for (a) and the c axis is out of the plane for (b) and (c).

$x=2.80$ sample displays a large drop in M/H at ~70 K, which indicates that this compound contains a fraction of the $Sr_8Fe_8O_{23}$ ($x=2.875$) phase. The other two oxygen contents

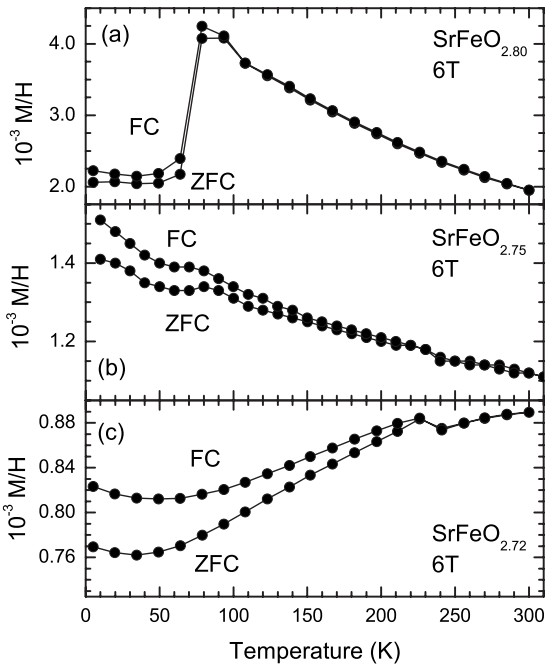

FIG. 2. Plot of the zero-field-cooled and field-cooled M/H data at 6 T from (a) $SrFeO_{2.80}$, (b) $SrFeO_{2.75}$, and (c) $SrFeO_{2.72}$.

have a M/H that is only weakly temperature dependent. There is a small increase in M/H for the $x=2.75$ sample as well as hysteresis behavior near the $Sr_4Fe_4O_{11}$ antiferromagnetic ordering temperature (~230 K). There is also a small feature near 70 K, which indicates that this sample contains a small fraction of the $Sr_8Fe_8O_{23}$ ($x=2.875$) phase. The $x=2.72$ sample shows hysteresis behavior near 230 K that can be attributed to a fraction of the $Sr_4Fe_4O_{11}$ ($x=2.75$) phase. There is no evidence in the $x=2.72$ M/H data for the $Sr_8Fe_8O_{23}$ ($x=2.875$) phase. Field-cooled measurements at lower applied fields (25 mT) show that all samples from $x=2.80$ to $x=2.72$ contain a fraction of the $Sr_4Fe_4O_{11}$ phase.

Magnetization data are plotted in Fig. 3(a) for $x=2.75$ at 10 K and as a function of the applied magnetic field after field cooling in applied magnetic fields of +5 or −5 T. The magnetization curves show weak hysteresis and the magnetization has not saturated even for applied magnetic fields of 6 T. Furthermore, the magnetization loops are symmetrically offset from the origin. A similar offset has been reported for temperatures below 230 K from measurements on $SrFeO_{2.83}$ where the Néel temperature was reported as being 120 K.[11] It was attributed to competing antiferromagnetic and ferromagnetic interactions in a helical spin system. However, we show in Fig. 3(b) that this offset can be attributed to the G-type antiferromagnet, $Sr_4Fe_4O_{11}$ ($x=2.75$). Here we plot magnetization curves at 10 K after field cooling in 5 T and for different oxygen contents. It can be seen that the biggest offset occurs for $x=2.75$. This is clearer in the inset where the offset field B_E is plotted as a function of the oxygen content from these and other samples.

Shifts in the magnetization curves away from the origin have also been observed in some spin glasses, nanophase magnetic materials, and films containing ferromagnetic and antiferromagnetic layers.[12–16] Most research effort has fo-

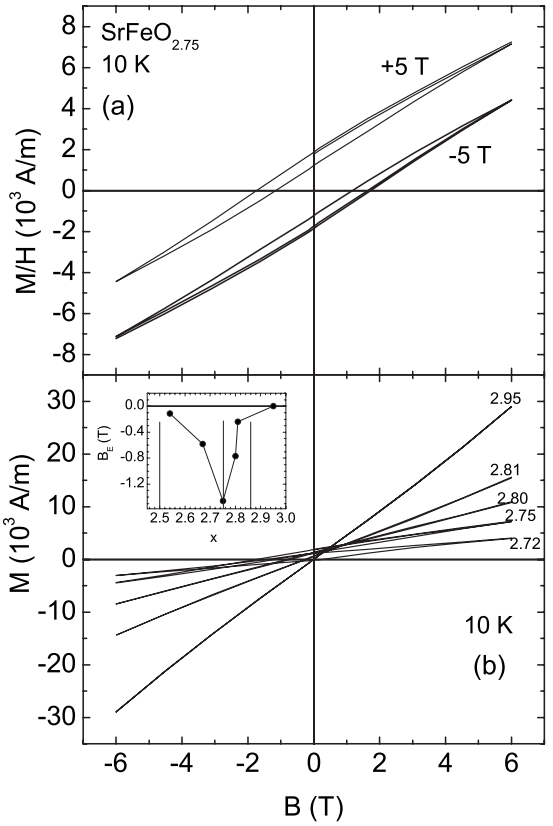

FIG. 3. (a) Plot of the magnetization against the applied magnetic field for $x=2.75$ at 10 K after cooling in an applied magnetic field of +5 or −5 T. (b) Plot of the magnetization against the applied magnetic field after field cooling to 10 K in an applied magnetic field of +5 T for $x=2.95$, 2.81, 2.80, 2.75, and 2.72. Inset: Plot of the offset field B_E against the oxygen content x. The vertical lines indicate the $Sr_2Fe_2O_5$ ($x=2.5$), $Sr_4Fe_4O_{11}$ ($x=2.75$), and $Sr_8Fe_8O_{23}$ ($x=2.875$) phases.

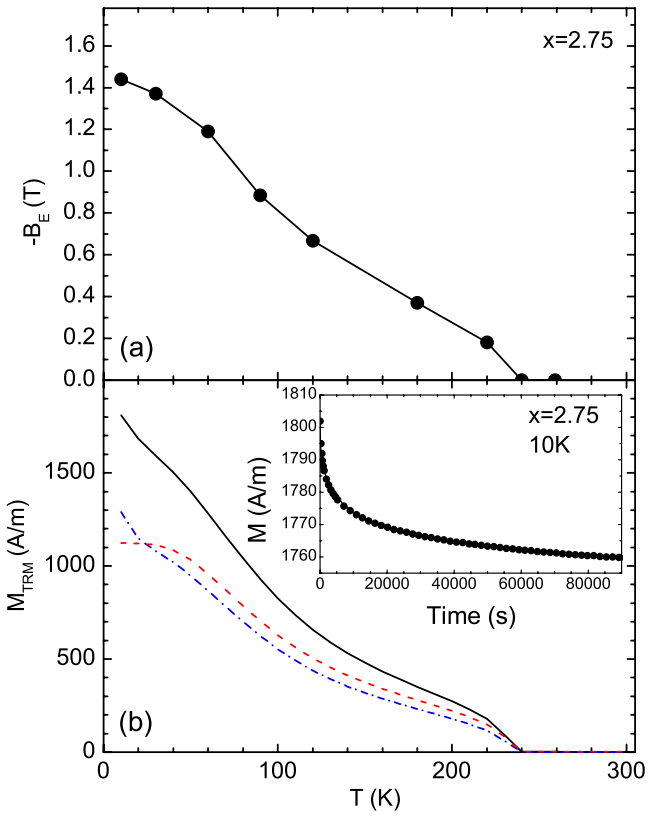

FIG. 4. (Color online) (a) Plot of the exchange-bias-like field B_E against temperature after cooling in a field of 6 T. (b) Plot of the thermoremnant magnetization M_{TRM} after field cooling to 10 K in a field of 5 T and then turning the field off, for $x=2.80$ (dot-dashed curve), $x=2.75$ (solid curve), and $x=2.72$ (dashed curve). Inset: Plot of M_{TRM} at 10 K against time after cooling in a field of 5 T and then turning the field off. The solid curve is a stretched exponential fit to the data.

cused on ferromagnetic/antiferromagnetic interfaces where there is an additional term in the magnetic energy density arising from exchange coupling between the ferromagnetic and antiferromagnetic spins at the interface. In the simplest case it is possible to show that this additional unidirectional anisotropy term leads to an exchange bias field of $B_E = \mu_0 \Delta\sigma / (M_{FM} t_{FM})$,[12,13] where $\mu_0 = 4\pi \times 10^{-7}$ N/A^2, $\Delta\sigma$ is the interfacial unidirectional energy density, M_{FM} is the saturated ferromagnetic moment, and t_{FM} is the thickness of the ferromagnetic layer. For spin glasses there can occur ferromagnetic and antiferromagnetic spin-glass clusters where the origin of B_E is similar to that in ferromagnetic/antiferromagnetic thin films. However, there are other possible effects such as those believed to occur in $Ni_{1-x}Mn_x$, where the nearest-neighbor exchange is believed to ferromagnetic and the next-nearest-neighbor exchange is believed to be antiferromagnetic. It has been argued that including a Dzyaloshinsky-Moriya term can result in unidirectional anisotropy and hence an exchange bias B_E.[14,15]

The situation in $Sr_4Fe_4O_{11}$ is more complicated because of Fe(1) moment spin frustration and Fe(2) moment antiferromagnetic order. Thus, B_E could possibly arise from Fe(1) spin-glass clusters. However, we show below that this can be discounted.

To further investigate the nature of the exchange-bias-like effect, we performed magnetization loop measurements on the $x=2.75$ sample at different temperatures after cooling in a field of 5 T. The resultant B_E is plotted in Fig. 4(a). It can be seen that B_E systematically decreases with decreasing temperature and disappears near the Fe(2) moment antiferromagnetic ordering temperature. This suggests that the exchange-bias-like effect originates from the antiferromagnetically ordered Fe(2) moments and exchange coupling to ferromagnetically ordered spins or a ferromagnetic spin glass.

The appearance of a spin glass is usually signaled by a frequency-dependent ac susceptibility χ', as well a time-dependent thermoremnant magnetization.[17] We have attempted ac-magnetization measurements with frequencies from 4 Hz to 1 kHz but there is no evidence for a frequency dependent χ' within the experimental uncertainty. This is probably because the magnitude of χ' is too small. However, there is a thermoremnant magnetization, as can be seen in Fig. 4(b). Here we plot the magnetization for $x=2.80$, 2.75, and 2.72 after cooling in a field of 5 to 10 K and then turning the field off. It can be seen that it is largest for the $x=2.75$ sample and disappears at the Fe(2) moment antiferromagnetic ordering temperature.

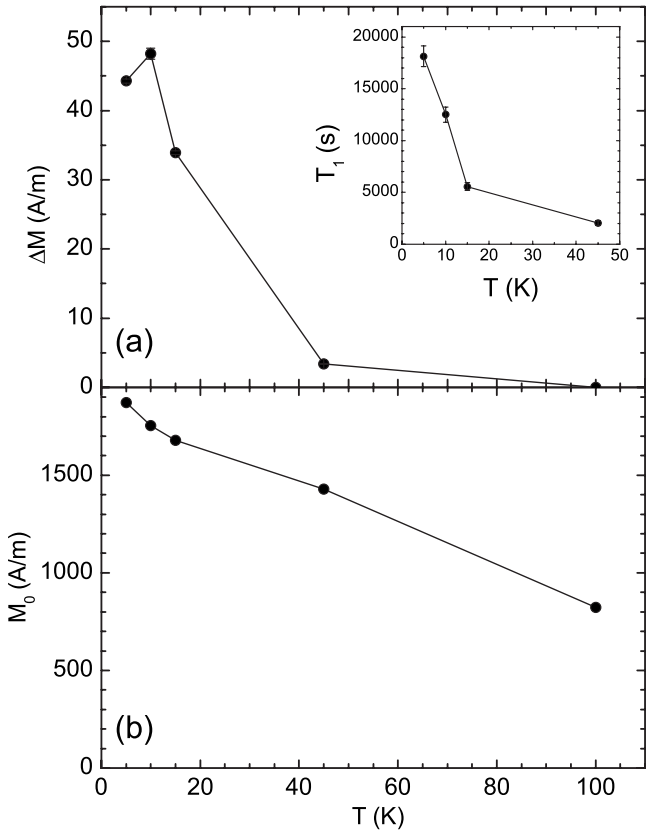

FIG. 5. Plots of (a) ΔM and (b) M_0 after fitting the $x=2.75$ thermoremnant magnetization data to the stretched exponential in the text. The inset of (a) shows the fitted T_1 against temperature.

The thermoremnant (TRM) magnetization M_{TRM} does display time dependence, as can be seen in the inset of Fig. 4(b). Here the magnetization is plotted after cooling to 10 K in an applied magnetic field of 5 T, turning off the field, and immediately starting the magnetization measurements. We find that the time dependence of M_{TRM} is not well described by $M_{\mathrm{TRM}} \propto t^{-n}$ that is based on an Ising spin-glass model, where t is the time.[18] Rather, the data are better described by the commonly used stretched exponential,[17,19–23]

$$M_{\mathrm{TRM}} = \Delta M \exp[-(t/T_1)^n] + M_0, \qquad (1)$$

where ΔM is the prefactor, T_1 is a characteristic relaxation time, n is the stretched exponential exponent, and M_0 is a constant. Ideally, M_0 should be zero. Equation (1) can be interpreted in terms of a distribution of relaxation rates, which is probably expected in a disordered magnetic system. It can be seen in the inset of Fig. 4(b) that Eq. (1) provides a good fit to the data where we find that $\Delta M=48$ A/m, $T_1=12\,500$ s, $n=0.39$, and $M_0=1755$ A/m. The low value of n indicates that there is a large distribution in the spin-glass relaxation rates. The parameters obtained after fitting the data taken at different temperatures can be seen in Fig. 5 where $n=0.39$ below 50 K.

The fitted ΔM and T_1 values are zero above ~50 K and ΔM is <3% of the time-independent component, M_0. ΔM can be attributed to a small spin-glass component, possibly arising from the Fe(1) moments, where the spin-glass temperature is ~50 K. The small $\Delta M/M_0$ ratio (<3%) would explain why no frequency-dependent ac magnetization could be observed within the experimental uncertainty. In this scenario the exchange-bias-like effect cannot simply be attributed to a Fe(1) moment spin-glass because the spin-glass component would need to be larger and observed for temperatures up to ~240 K where B_E disappears.

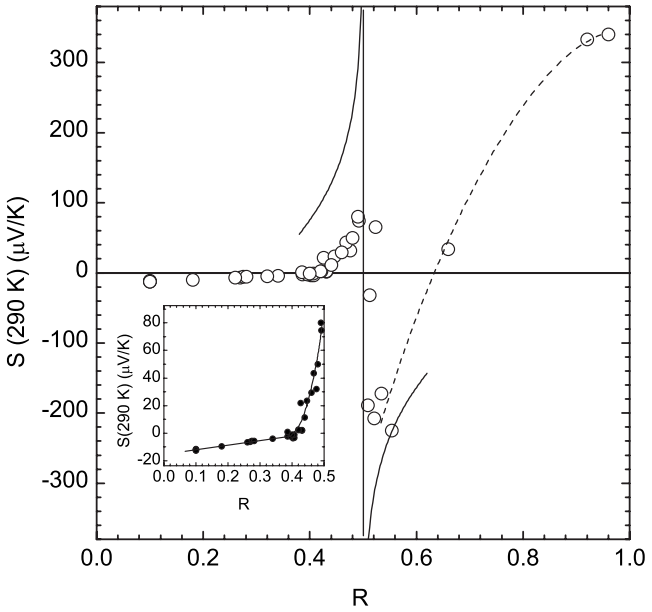

FIG. 6. Plot of the room-temperature thermopower against R, where $4-R$ is the average Fe valence. The vertical line indicates the stoichiometric $Sr_4Fe_4O_{11}$ ($x=2.75$) phase. Also shown is the Heikes formula (solid curve). The dashed curve is a guide for the eyes. Inset: Expanded view of the room-temperature thermopower for R between 0 and 0.5. The solid curve is a guide for the eyes.

The appearance of B_E and M_0 for temperatures below the Fe(2) moment Néel temperature clearly indicates that at least the Fe(2) moments are partly responsible. However, the interactions that lead to the exchange-bias-like effect are not clear.

We now discuss the results from room-temperature thermopower measurements. In Fig. 6 the room-temperature thermopower, $S(290\ \mathrm{K})$, is plotted against R obtained from the average Fe valence, Fe^{4-R}, where $x=3-R/2$. For small values of R (i.e., for x near 3), $S(290\ \mathrm{K})$ is small and negative. For $x=2.95$, we find that $S(290\ \mathrm{K})$ is $\sim -10\ \mu\mathrm{V/K}$, which is indicative of n-type conduction but it is too large for a simple metal. This shows the complex nature of charge transport in this compound. As R increases (i.e., x decreases) there is a systematic increase in $S(290\ \mathrm{K})$ to positive values and there is a sudden change in sign at $R=0.5$. This corresponds to the $Sr_4Fe_4O_{11}$ ($x=2.75$) phase. The dependence of $S(290\ \mathrm{K})$ on R for $R<0.5$ is seen more clearly in the inset of Fig. 6. It also shows that $S(290\ \mathrm{K})$ can be used to estimate R and hence x in situations where x is not known. Similar $S(290\ \mathrm{K})$ correlations have already been very useful in estimating the average Cu valance in the CuO_2 planes in high-temperature superconducting cuprates.[24] As R increases from 0.5 to 1.0, $S(290\ \mathrm{K})$ decreases from a large negative value to a large positive value.

A sudden change in the sign of the high-temperature thermopower has been observed in some other transition-metal oxides[25–27] and it has been modeled using the Heikes formula.[28–30] For example, it has been used to model the change in sign of the room-temperature thermopower in electron-doped $La_{1-x}Sr_xCoO_3$.[30]

The room-temperature thermopower from $La_{1-x}Sr_xCoO_3$ was interpreted by first noting that it can be shown in the Hubbard model that for a narrow band in the high-temperature limit, the thermopower can be written as[30]

$$S = -\frac{k_B}{e}\frac{\partial \ln(g)}{\partial N}, \tag{2}$$

where g is the total number of configurations and k_B is Boltzmann's constant. Electron doping in $La_{1-x}Sr_xCoO_3$ has been modeled in terms of a changing concentration of Co^{3+} and Co^{4+}. Thus, by determining the total number of possible configurations it can be shown from Eq. (2) that the high-temperature limit of the thermopower can be described by the Heikes formula, which can be written as[30]

$$S = -\frac{k_B}{e}\ln\left(\frac{g_3}{g_4}\frac{y}{1-y}\right), \tag{3}$$

where y is the fraction of Co^{4+} ions and g_3 and g_4 are the total numbers of electronic configurations of Co^{3+} and Co^{4+}, respectively.

The situation in $Sr_4Fe_4O_{11}$ is more complicated because it contains 50% Fe^{4+} and 50% Fe^{3+}. Thus, hole doping close to $x=2.75$ ($R=0.5$) could be considered to occur by an increasing fraction of Fe^{4+} on the Fe site that has a valence of 3+ in $Sr_4Fe_4O_{11}$. In one interpretation, this would correspond to increasing the Fe(2) valence from 3+ to 4+.[6] For convenience, we take the interpretation where the Fe(1) valence is 4+ and the Fe(2) valence is 3+ when $x=2.75$.[6] Note, that choosing the other interpretation will not affect the results. Thus, the total number of possible configurations, g, is

$$g = g_3^{N_0-M_e} g_4^{M_e} \frac{N_0!}{M_e!\,(N_0-M_e)!}, \tag{4}$$

where N_0 is the total number of Fe^{3+} sites when $x=2.75$, which corresponds to the total number of Fe(2) sites. M_e is the excess number of Fe^{4+} ions on the Fe(2) sites. g_3 and g_4 are the number of Fe^{3+} and Fe^{4+} configurations, respectively. By comparison with similar studies on compounds containing Co (Ref. 30) and Mn,[31] we take $g_3=6$ and $g_4=10$ for the high spin configurations. Thus, from Eqs. (3) and (4) it is possible to show that

$$S = -\frac{k_B}{e}\ln\left(\frac{g_3}{g_4}\frac{z_1}{1-z_1}\right), \tag{5}$$

where $z_1=M_e/N_0=1-2R$. A similar approach can be taken for the case where there is electron doping close to $x=2.75$ ($R=0.5$). This will lead to

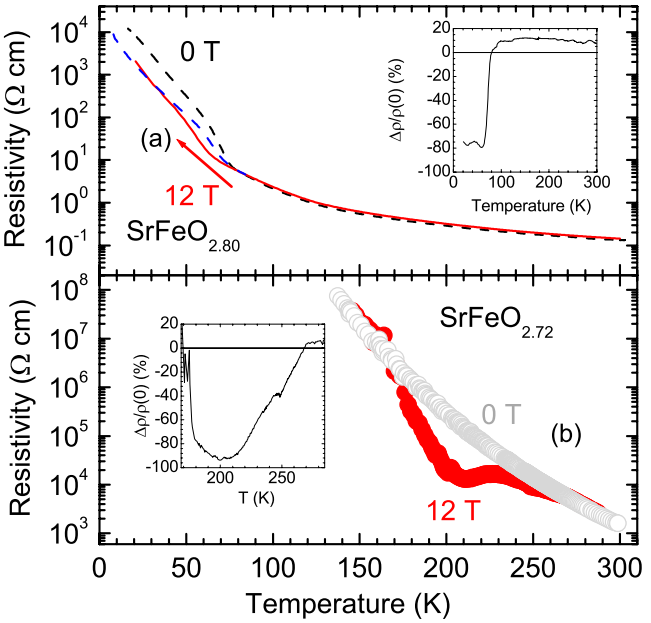

FIG. 7. (Color online) (a) Plot of the resistivity against temperature when cooling from 300 K for zero applied field (upper dashed black curve) and in an applied magnetic field of 12 T (solid red curve) for $x=2.80$. Also shown is the high-field resistivity when warming (lower dashed blue curve). The inset is a plot of the magnetoresistance when cooling from 300 K. (b) Plot of the resistivity against temperature for zero applied field (gray open circles) and in an applied magnetic field of 12 T (filled circles) $x=2.72$. The inset is a plot of the magnetoresistance.

$$S = +\frac{k_B}{e}\ln\left(\frac{g_4}{g_3}\frac{z_2}{1-z_2}\right), \tag{6}$$

where $z_2=2R-1$, N_0 is now the total number Fe(1) sites, and M_e is the excess number of Fe^{3+} ions on the Fe(1) sites.

It can be seen in Fig. 6 (solid curves) that Eqs. (5) and (6) provide a qualitative description of the data. However, it should be noted that Eqs. (5) and (6) are only reasonable for oxygen contents close to 2.75. This is because samples with x values on either side of 2.75 will also contain a mixture of the $x=2.875$ or $x=2.5$ phases. This can lead to a much faster decrease in the absolute values of $S(290\ \mathrm{K})$ for x above or below 2.75.

High-field resistivity measurements were done on two samples and the results can be seen in Fig. 7(a) for $x=2.80$ and Fig. 7(b) for $x=2.72$. The $x=2.80$ sample displays an increase in the resistivity for temperatures below ~70 K that is likely to arise from a fraction of the $Sr_8Fe_8O_{23}$ ($x=2.875$) phase. This is because the $Sr_8Fe_8O_{23}$ ($x=2.875$) phase is known to display a large increase in the resistivity near the Néel temperature and associated with partial charge ordering on one of the Fe sites.[1,2] Similar to two previous studies,[1,2] we observe a temperature-dependent irreversibility at high fields near the $Sr_8Fe_8O_{23}$ ($x=2.875$) phase Néel temperature. However, unlike previous measurements on single-crystal samples for $x=2.81$,[1,2] we find that the resistivity is also lower for temperatures far below ~70 K and for an applied magnetic field of 12 T. The resultant magne-

toresistance is plotted in the inset of Fig. 7(a) as $\Delta\rho/\rho=[\rho(12\ \mathrm{T})-\rho(0)]/\rho(0)$. It is not clear why large negative $\Delta\rho/\rho$ values occur down to low temperatures when compared with the results from single-crystal samples with $x=2.81$ where negative $\Delta\rho/\rho$ values are observed between ~30 and 70 K and positive $\Delta\rho/\rho$ values are observed below ~30 K.[1] The difference could be due to an additional magnetoresistance contribution from transport across the grain boundaries. However, this would appear to be unlikely because our resistivity values are below those measured in the $x=2.81$ single crystal at 300 K and comparable with the single-crystal resistivities at low temperatures.

The $x=2.72$ sample displays a semiconductinglike resistivity in zero applied field [Fig. 7(b)], and the resistivity is significantly reduced in an applied magnetic field of 12 T for temperatures below ~270 K. This temperature is near the $Sr_4Fe_4O_{11}$ ($x=2.75$) Néel temperature and hence it is possible that it is associated with this phase fraction. A very large magnetoresistance is observed at 12 T, which is clearer in the inset where $\Delta\rho/\rho$ is plotted. Unfortunately, we cannot compare our results with those on single-crystal samples because there are no reports of magnetoresistance measurements on single crystals with similar oxygen contents. It is possible that the very large $\Delta\rho/\rho$ is dominated by intergrain transport.

IV. CONCLUSION

In conclusion, we have performed magnetization and transport measurements on $SrFeO_{3-x}$ for oxygen contents about the orthorhombic $Sr_4Fe_4O_{11}$ ($x=2.75$) phase. There is evidence for a spin glass for temperatures below ~50 K that could be due to the spin-frustrated Fe(1) moments in the $Sr_4Fe_4O_{11}$ phase fraction. We find an exchange-bias-like effect that can be attributed to the $Sr_4Fe_4O_{11}$ phase, although the physical origin of this effect is not clear. The exchange-bias-like effect commences at the $Sr_4Fe_4O_{11}$ Néel temperature where the Fe(2) moments antiferromagnetically order. This indicates that the Fe(2) moments are somehow involved. However, the exchange-bias-like effect is unlikely to originate from a spin glass because the spin-glass temperature (~50 K) is significantly below the temperature where the exchange-bias-like effect commences (~240 K). The room-temperature thermopower displays a large change in sign for oxygen contents on either side of $x=2.75$ that can be qualitatively interpreted using the Heikes formula for x values close to 2.75. This suggests that the Fermi level is within a narrow band. A very large magnetoresistance is found for $x=2.72$ below ~260 K that could arise from the $Sr_4Fe_4O_{11}$ phase fraction.

ACKNOWLEDGMENTS

The authors acknowledge funding from the New Zealand Foundation for Research Science and Technology, the New Zealand Marsden Fund, and the MacDiarmid Institute. They thank R. Gaál and L. Forró for the provision of the transport facility at the École Polytechnique Fédéral de Lausanne, and M. Bowden for producing the structural diagrams.

[1] A. Lebon, P. Adler, C. Bernhard, A. V. Boris, A. V. Pimenov, A. Maljuk, C. T. Lin, C. Ulrich, and B. Keimer, Phys. Rev. Lett. **92**, 037202 (2004).
[2] P. Adler, A. Lebon, V. Damljanovic, C. Ulrich, C. Bernhard, A. V. Boris, A. Maljuk, C. T. Lin, and B. Keimer, Phys. Rev. B **73**, 094451 (2006).
[3] T. Takeda, Y. Yamaguchi, and H. Watanabe, J. Phys. Soc. Jpn. **33**, 967 (1972).
[4] Y. M. Zhao, R. Mahendiran, N. Nguyen, B. Raveau, and R. H. Yao, Phys. Rev. B **64**, 024414 (2001).
[5] P. K. Gallagher, J. B. MacChesney, and D. N. E. Buchanan, J. Chem. Phys. **41**, 2429 (1964).
[6] J. P. Hodges, S. Short, J. D. Jorgensen, X. Xiong, B. Dabrowski, S. M. Mini, and C. W. Kimball, J. Solid State Chem. **151**, 190 (2000).
[7] E. K. Hemery, G. V. M. Williams, and H. J. Trodahl, Phys. Rev. B **75**, 092403 (2007).
[8] M. Schmidt, M. Hofmann, and S. J. Campbell, J. Phys.: Condens. Matter **15**, 8691 (2003).
[9] R. Vidya, P. Ravindran, H. Fjellvag, and A. Kjekshus, Phys. Rev. B **74**, 054422 (2006).
[10] S. Nakamura and S. Iida, Jpn. J. Appl. Phys., Part 2 **34**, L291 (1995).
[11] S. Srinath, M. Mahesh Kumar, M. L. Post, and H. Srikanth, Phys. Rev. B **72**, 054425 (2005).
[12] A. E. Berkowitz and K. Takano, J. Magn. Magn. Mater. **200**, 552 (1999).
[13] J. Nogués and I. K. Schuller, J. Magn. Magn. Mater. **192**, 203 (1999).
[14] J. S. Kouvel, W. Abdul-Razzaq, and Kh. Ziq, Phys. Rev. B **35**, 1768 (1987).
[15] Kh. A. Ziq and J. S. Kouvel, Phys. Rev. B **41**, 4579 (1990).
[16] D. Mauri, H. C. Siegmann, P. S. Bagus, and E. Kay, J. Appl. Phys. **62**, 3047 (1987).
[17] K. Binder and A. P. Young, Rev. Mod. Phys. **58**, 801 (1986).
[18] S. Kirkpatrick and D. Sherrington, Phys. Rev. B **17**, 4384 (1978).
[19] R. Hoogerbeets, Wei-Li Luo, and R. Orbach, Phys. Rev. B **34**, 1719 (1986).
[20] G. C. DeFotis, G. S. Coker, J. W. Jones, C. S. Branch, H. A. King, J. S. Bergman, S. Lee, and J. R. Goodey, Phys. Rev. B **58**, 12178 (1998).
[21] J. Lago, P. D. Battle, and M. J. Rosseinsky, J. Phys.: Condens. Matter **12**, 2505 (2000).
[22] M. D. Mukadam, S. M. Yusuf, P. Sharma, S. K. Kulshreshtha, and G. K. Dey, Phys. Rev. B **72**, 174408 (2005).
[23] C. Jaeger, C. Bihler, T. Vallaitis, S. T. B. Goennenwein, M. Opel, R. Gross, and M. S. Brandt, Phys. Rev. B **74**, 045330 (2006).
[24] J. L. Tallon, J. R. Cooper, P. S. I. P. N. de Silva, G. V. M. Williams, and J. W. Loram, Phys. Rev. Lett. **75**, 4114 (1995).

[25] A. Maignan, D. Flahaut, and S. Herbert, Eur. Phys. J. B **39**, 145 (2004).
[26] K. Berggold, M. Kriener, C. Zobel, A. Reichl, M. Reuther, R. Muller, A. Freimuth, and T. Lorenz, Phys. Rev. B **72**, 155116 (2005).
[27] A. A. Taskin, A. N. Lavrov, and Yoichi Ando, Phys. Rev. B **73**, 121101(R) (2006).
[28] R. R. Heikes and R. W. Ure, Jr., *Thermoelectricity: Science and Engineering* (Interscience, New York, 1961).
[29] P. M. Chaikin and G. Beni, Phys. Rev. B **13**, 647 (1976).
[30] W. Koshibae, K. Tsutsui, and S. Maekawa, Phys. Rev. B **62**, 6869 (2000).
[31] W. Kobayashi, I. Terasaki, M. Mikami, R. Funahashi, T. Nomura, and T. Katsufuji, J. Appl. Phys. **95**, 6825 (2004).